Accepted Manuscript

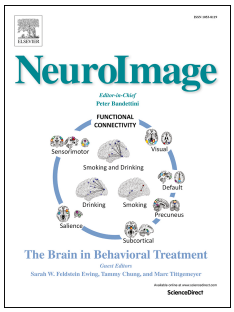

Functionally dissociating ventro-dorsal components within the rostro-caudal hierarchical organization of the human prefrontal cortex

F.K. Schumacher, L.V. Schumacher, B.O. Schelter, C.P. Kaller

PII: S1053-8119(18)32020-2

DOI: 10.1016/j.neuroimage.2018.10.048

Reference: YNIMG 15367

To appear in: *NeuroImage*

Received Date: 27 August 2018

Revised Date: 16 October 2018

Accepted Date: 17 October 2018

Please cite this article as: Schumacher, F.K., Schumacher, L.V., Schelter, B.O., Kaller, C.P., Functionally dissociating ventro-dorsal components within the rostro-caudal hierarchical organization of the human prefrontal cortex, *NeuroImage* (2018), doi: https://doi.org/10.1016/j.neuroimage.2018.10.048.

Functionally dissociating ventro-dorsal components within the rostro-caudal hierarchical organization of the human prefrontal cortex

Abbreviated title: Separating rostro-caudal gradients in the PFC

F.K. Schumacher[1,2,3,5,6], L.V. Schumacher[1,2,4,5,6], B.O. Schelter[6,7], C.P. Kaller[1,2,5,6]

[1] Dept. of Neurology, Medical Center – University of Freiburg, 79106 Freiburg, Germany | [2] Freiburg Brain Imaging Center, University of Freiburg, 79106 Freiburg, Germany | [3] Faculty of Biology, University of Freiburg, 79104 Freiburg, Germany | [4] Medical Psychology and Medical Sociology, University of Freiburg, 79104 Freiburg, Germany | [5] Faculty of Medicine, University of Freiburg, 79085 Freiburg, Germany | [6] BrainLinks-BrainTools Cluster of Excellence, University of Freiburg, 79110 Freiburg, Germany | [7] Institute for Complex Systems and Mathematical Biology, University of Aberdeen, Aberdeen AB24 3UE, UK

Corresponding author: Dr. Christoph Kaller (christoph.kaller@uniklinik-freiburg.de)
Dept. of Neurology, Medical Center - University of Freiburg,
Breisacher Str. 64, 79106 Freiburg, Germany

Number of pages: 26

Number of figures: 5

Number of words: Abstract: 249/250; Introduction: 621/650; Discussion: 1313/1500

Conflicts of interest: The authors declare no competing financial interests.

Acknowledgement: This work was supported by a grant of the BrainLinks-BrainTools Cluster of Excellence funded by the German Research Foundation (DFG, grant number EXC 1086).

Abstract (250/250words)

Cognitive control is proposed to rely on a rostral-to-caudal hierarchy of neural processing within the prefrontal cortex (PFC), with more rostral parts exerting control over more caudal parts. Anatomical and functional data suggest that this hierarchical organization of the PFC may be separated into a ventral and a dorsal component. Furthermore, recent studies indicate that the apex of the hierarchy resides within the mid-lateral rather the rostral PFC. However, investigating the hierarchical aspect of rostro-to-caudal processing requires quantification of the directed interactions between PFC regions.

Using functional near-infrared spectroscopy (fNIRS) in a sample of healthy young adults we analyzed directed interactions between rostral and caudal PFC during passive watching of nature documentaries. Directed coherence (DC) as a measure of directed interaction was computed pairwise between 38 channels evenly distributed over the lateral prefrontal convexity.

Results revealed an overall predominance of rostral-to-caudal directed interactions in the PFC that further dissociated along a ventro-dorsal axis: Dorsal regions exerted stronger rostro-caudally directed interactions on dorsal than on ventral regions and vice versa. Interactions between ventral and dorsal PFC were stronger from ventral to dorsal areas than vice versa. Results further support the notion that the mid-dorsolateral PFC constitutes the apex of the prefrontal hierarchy.

Taken together these data provide novel evidence for parallel dorsal and ventral streams within the rostro-caudal hierarchical organization of the PFC. FNIRS-based analyses of directed interactions put forward a new perspective on the functional architecture of the prefrontal hierarchy and complement previous insights from functional magnetic resonance imaging.

Significance Statement

The capabilities of the human prefrontal cortex (PFC) are a unique feature of our species, but our understanding of its functional principles is still vague. A theory currently under debate sheds light on how the PFC gives rise to the human cognition and goal-directed behavior. It assumes that abstract ideas are successively concretized into actual actions by processing relevant information along a rostro-caudal gradient in the PFC. Here we introduce a novel approach that is particularly promising for the assessment of the neurophysiological mechanisms in the PFC underlying the hierarchical control of behavior. Our results provide evidence for the rostro-caudally directed interplay within the PFC and quantify the interactions between the ventral and dorsal components of this hierarchical organization.

Introduction

Within the lateral prefrontal cortex (PFC), different levels of cognitive control are assumed to be hierarchically organized along a rostro-caudal axis, with rostral parts of the PFC performing highly abstract levels of behavioral control and caudal parts carrying out concrete action selection in a temporally confined context (Badre et al., 2009; Blumenfeld et al., 2013; Koechlin et al., 2003, 1999; Voytek et al., 2015). Evidence for this hierarchical organization of neural processing has been provided by task-based functional magnetic resonance imaging (fMRI) studies (Badre & D'Esposito, 2007; Bahlmann, Blumenfeld, & D'Esposito, 2015; Koechlin et al., 1999, for a review see Badre & D'Esposito, 2009) but is also supported by lesion data (Azuar et al., 2014) and transcranial magnetic stimulation (Nee and D'Esposito, 2017). However, other studies showed that rostral PFC regions can also be recruited by concrete action selection (Crittenden and Duncan, 2014) and that the temporal, rather than the spatial activation profile of specific PFC regions is modulated by maintenance demands, irrespective of the level of abstraction (Reynolds et al., 2012). Tracer studies in monkeys further demonstrated that the structural network in the PFC does not follow a strict rostro-caudal organization (Goulas et al., 2014). The extent to which the PFC is organized along a rostro-caudal axis hence constitutes a matter of debate.

Beyond functional gradients along a rostro-caudal axis, the structural and functional organization of the PFC has also been subject to anatomically detailed characterizations along a ventro-dorsal axis (see Tanji & Hoshi, 2008 and Petrides, 2005 for reviews). In this respect, it has been demonstrated that potentially separable rostro-caudal streams of processing are present in the ventral and dorsal convexity of the lateral PFC (Blumenfeld et al., 2018, 2013). Using a resting-state fMRI paradigm, Blumenfeld et al. (2013) found parallel ventral and dorsal networks that were interconnected in caudal but not in rostral PFC regions. Bahlmann et al. (2015) further suggested that rostro-caudally organized functional networks in ventral and dorsal PFC adapt their ventro-dorsal segregation dynamically to be operative on the highest level of the rostro-caudal axis that is currently engaged in the task, whereas on lower levels processing is integrated across ventral and dorsal areas. The lateral PFC thus seems to comprise parallel rostro-caudal pathways which appear anatomically separable along a ventro-dorsal axis but functionally interact to subserve goal-directed behavior. While this functional interaction has

been proposed to be orchestrated by the rostral-most part of the lateral PFC (e.g. Ramnani and Owen, 2004; Wendelken et al., 2012; for a recent review on the function of the frontopolar cortex see Mansouri et al., 2017), recent evidence suggests that the apex of the prefrontal hierarchy actually resides in the mid-lateral rather than the rostral PFC (Margulies et al., 2016; Nee and D'Esposito, 2016; for a review see Badre and Nee, 2018).

Taken together, an abundance of fMRI studies demonstrate the gradual activation along the rostro-caudal and the ventro-dorsal axes of the PFC by task-related factorial designs (e.g., Bahlmann et al., 2015) as well as the functional connectivity, between the respective regions by correlation analyses of resting-state activity (e.g. Taren et al., 2011). These studies argue for a hierarchical functional organization of the PFC. However, to fully understand the mechanisms and functional pathways that subserve cognitive functions requires to complement these correlation- and activation-based analyses by the inference of the actual direction of influences and the demonstration of the implied propagation of neural activity along a rostro-to-caudal gradient of hierarchical control within the lateral PFC. While the slow hemodynamic response is well captured by sampling intervals between 0.5 and 2 Hz as provided by conventional fMRI (Logothetis, 2008), functional interactions between brain regions appear on a much smaller temporal scale (Stokes et al., 2013). Reliably inferring *directed* functional connections from such very short delays between neural activity in different regions requires much faster sampling of at least 10 Hz (Mader et al., 2008; Roebroeck et al., 2005). Simplifying the problem of inferring directionality down to the detection of short delays between oscillations (Granger, 1969), the need for a sufficiently high temporal resolution can be easily illustrated by plotting two noisy sine waves with a small phase shift using different sampling rates. A phase shift which is entirely obscure when sampled at .5 Hz can become highly apparent when sampled at 10 Hz (Supplementary Figure S1).

Similar to fMRI, functional near-infrared spectroscopy (fNIRS) relies on the neuro-vascular coupling and measures the hemodynamic response but in contrast to fMRI it is based on the differential absorption properties of oxygenated and deoxygenated hemoglobin (Scholkmann et al., 2014; Strangman et al., 2002). Multiple light sources and detectors transcranially measure absorption

changes elicited by changes in cortical oxygenation at sample frequencies up to 250 Hz (Scholkmann et al., 2014). Thus, fNIRS overcomes the limited temporal resolution of fMRI and provides sufficiently high spatial resolution (here 2.1 cm) to allow for inference of *directed* functional interactions along rostro-caudal and ventro-dorsal axes in the PFC.

Here we used fast optical imaging with multi-channel fNIRS and measures of directed coherence (DC) (Schelter et al., 2006) to estimate the propagation of neural activity across the PFC and to provide complementary evidence for the predicted influences within and between parallel rostro-caudal signaling pathways in the ventral and dorsal PFC (Bahlmann et al., 2015; Blumenfeld et al., 2013; Bunge et al., 2005; Wendelken et al., 2012). We expected to reveal (i) a predominant rostral to caudal direction of influences within the PFC and (ii) a separation into a ventral and a dorsal component.

Methods

Experimental Design

Subjects between 19 and 26 years of age were recruited from the University of Freiburg provided that they were German native speakers and fulfilled MRI safety criteria. Exclusion criteria concerned current or previous psychiatric/neurological disease, use of psychotropic medication, and color blindness. Thirty-one subjects participated in two 24-minutes fNIRS measurements (one week apart) and additionally underwent MRI and neuropsychological assessments that were conducted as a part of a larger methodological study (see Köstering et al., 2015; Schumacher et al., 2018). Depressive symptoms were screened for with the Beck Depression Inventory-II (BDI-II; Beck, Steer, & Brown, 1996), and MR images were inspected for incidental findings. All subjects were right-handed, had normal or corrected-to-normal vision, received a compensation of 60 €, and gave written informed consent to participation. The study was approved by local ethics authorities. As two subjects had to be excluded (one BDI-II score of 15 indicating mild depressivity (Beck et al., 1996), one incidental MRI finding), the final sample comprised 29 subjects (age, mean ± standard deviation 22.6±1.8 years; 13 males; all university students).

Functional near-infrared spectroscopy measurements (fNIRS)

FNIRS measurements were conducted using an ETG-4000 optical topography system (Hitachi Medical Systems, Japan) which provides a sampling frequency of 10 Hz and operates in a continuous wave mode with two different wavelengths of near-infrared light (695 nm and 830 nm). Spatial optode arrangement was derived from the system's 3×11 grid configuration consisting of 17 emitters and 16 detectors. We modified this probe set by placing 12 emitters and 13 detectors on the forehead (interoptode distance of 3 cm), thus resulting in 38 channels evenly distributed over the lateral PFC (cf. Fig. 4). The modified probe set comprised 3 further emitter-detector-pairs with a smaller interoptode distance of approximately 1.8 cm which were placed on the parietal bone but not included in the present analyses. Three unused emitter optodes were covered by a black cap to avoid crosstalk. Grid placement over PFC was standardized across subjects (i) by aligning its center optodes to the sagittal midline and (ii) by positioning the lower center optode at a distance of about 1.5 cm above the nasion.

Data were acquired for 24 minutes in a task-free state. Subjects watched two different muted nature documentaries on both testing sessions (selected scenes without text overlays from "Earth", Fothergill & Linfield, 2007). The order of scenes was balanced across subjects. Muted videos were presented instead of a fixation cross (i) in order increase comfort for and compliance of participants and (ii) because specificity of functional connectivity has been shown to be higher during natural viewing conditions than during 'pure' rest (Bartels and Zeki, 2005). Presentation of the nature documentaries and on-/offset of simultaneous fNIRS recording were controlled by NBS Presentation software (version 12.2; Neurobehavioral Systems Inc., CA). Following a short interval of baseline fNIRS measurements, temporal markers were automatically set for later identification of the 24 minutes time window within the fNIRS time series that corresponded to an identical section of the videos across all subjects. To prevent artifacts during fNIRS measurement due to head movements, subject's head was stabilized using a chin rest.

Raw data of light intensity changes were converted into hemoglobin concentration changes by in-house Matlab software (version 2012b, The MathWorks, Natick, MA, USA, Kaller, Schumacher,

Schelter, unpublished toolbox) using the modified Beer-Lambert law (Cope and Delpy, 1988). Due to the absorption of interfering hairs some channels did not contain any signal. The respective time series were interpolated from the surrounding channels using the Matlab 4 griddata method. With respect to all recorded channels included in the analyses, this affected a total of 29 out of 1865 channels (1.56 %). Note that treating the 2.75% of connections that involved interpolated channels as missing data in the respective statistical models revealed virtually identical results. In order to remove motion-induced artifacts, we applied the correlation-based correction method developed by Cui, Bray, & Reiss (2010). The resulting data for oxygenated and deoxygenated hemoglobin are perfectly anticorrelated and therefore have identical spectral properties. No further preprocessing was applied to avoid bias of the connectivity estimates (Florin et al., 2010).

Spatial reconstruction of fNIRS channel positions

Optode locations and irradiation were recorded in an independent sample of 20 healthy adults (mean age ± standard deviation: 24.6 ± 2.8 years) using a PATRIOT digitizer (Polhemus Inc., VT) and custom-built software. Recording included the locations of three fiducials (nasion, left/right preauricular points) and a scattered point-wise sampling of the head surface. Reconstruction of optode positions was accomplished by co-registration of the surface points with the individual anatomical MRI scans (T1-weighted MPRAGE images acquired on a 3T Tim Trio scanner; Siemens AG, Erlangen, Germany; scan acquisition parameters: repetition time, 2200 ms; echo time, 2.15 ms; inversion time, 1100 ms; flip angle, 12°; 160 sagittal slices; matrix size, 256×256; field of view, 256 mm, resulting in 1.0 mm^3 cubic voxels), based on iterative closest point procedure. Segmentation of structural MRI scans was performed using the 'new segment' approach implemented in SPM8 (http://www.fil.ion.ucl.ac.uk/spm/software/spm8/) with default prior maps for gray matter, white matter, cerebro-spinal fluid, and three non-brain tissue classes. The segmented brain tissues were further used to create a normalized brain template based on the high-dimensional DARTEL (diffeomorphic anatomical registration through exponentiated lie algebra) approach (Ashburner, 2007). Individual fNIRS channel positions were calculated using the mean Euclidian distance of both the positions and the irradiation angles of the respective pairings of emitter and detector optodes (Supplementary Figure S2). Based on the deformation fields from the DARTEL normalizations, NIRS

channel positions on brain surface were then transformed into the sample-specific template space. The resulting individual channel positions and the group-averaged Euclidian mean positions are shown in Supplementary Figure S3. The group-averaged Euclidian mean channel positions were used for illustration of the spatial distribution of directed interactions by applying a 3D Gaussian smoothing kernel (3 cm full width at half maximum; Supplementary Figure S2) and rendering of the resulting kernel volume on the cortical surface (cf. Fig. 4). The Matlab code used for the spatial reconstruction of fNIRS channels and the visualization of the channel data on the cortical surface are available upon request.

Directed coherence as a measure of directed interactions between fNIRS channels

Directed interactions were estimated by means of directed coherence (DC) using the frequency domain multivariate analyses (FDMA) toolbox (www.fdm.uni-freiburg.de/Toolboxes/fdma-toolbox). As indicated by the term coherence, DC is a frequency-domain measure and is calculated by fitting a vector autoregressive model and transforming the estimated autoregression coefficients into the frequency domain (for details see Schelter et al., 2006). Thus, DC estimated from fNIRS data represents the strength and the direction of influences exerted between cortical areas in a certain frequency. The vector autoregressive model was fitted with a model order of 20, corresponding to the past 2 seconds of the time-series. As functional connectivity is apparent in low frequency oscillations (Biswal et al., 1995; Lowe et al., 2000), we chose the frequency band between .06 and .12 Hz and used the maximum DC value in this band for further analysis. Note that this approach is different from applying a band-pass filter during data preprocessing (which would potentially bias DC estimates (Florin et al., 2010)).

Statistical Analysis

Given the nested structure of the present data, DC values were analyzed in linear mixed effects models in R (version 3.4.2 (R Core Team, 2016)) using the lme4 package (version 1.1-14 (Bates et al., 2015)). In each hemisphere 16 channels in 4 streams along the rostro-caudal axis of the PFC were selected for analysis: 2 streams representing ventral and 2 streams representing dorsal PFC (Fig. 1). From all available channels, 2 channels located on the longitudinal fissure were excluded and another 2

channels per hemisphere were excluded in order to facilitate a balanced factorial design. Models were fitted with a random intercept for the interaction between the factors identifying the stream of the source channel, hemisphere, session and participant using maximum likelihood estimation.

Differences of influences between rostral and caudal as well as between and within ventral and dorsal streams were assessed in Model #1 with the following three fixed factors (Fig. 1) and all resulting interactions between them: direction (directed interactions from *rostral toward caudal* and from *caudal toward rostral* PFC), congruence (directed interactions *within* and *between* the ventral and dorsal streams), and level (three levels: the *rostral*, *middle*, and *caudal* connection between the selected channels along the rostro-caudal axis). In order to analyze differences between the ventral and the dorsal channels as the sources of influence, in Model #2 we fitted another mixed effects model considering only rostro-caudally directed influences and including (in place of direction) the factor source which distinguished whether the influence was exerted *by a ventral* or *by a dorsal* channel (Fig. 1). In correspondence with Model #1, the factors level and congruence as well as all possible interactions were also implemented in Model #2. Taken together, Model #1 assessed the rostro-caudal asymmetry of directed interactions and the degree of segregation between the ventral and the dorsal convexity, whereas Model #2 focused on the ventro-dorsal asymmetry of directed interactions within the rostro-caudal processing hierarchy.

Positions of the 16 selected channels, the considered influences and the fixed factors included in these two models are illustrated in Figure 1 for the left hemisphere. Significance of fixed effects were assessed using the anova method (Type III F-statistics with Satterthwaite's approximation of degrees of freedom) implemented in the lmerTest package (Kuznetsova et al., 2016) (version 2.0-33). Post-hoc comparisons and calculation of confidence bands were performed using the lsmeans package (Lenth, 2016) (version 2.27-2). Multiplicity was adjusted using Tukey’s method.

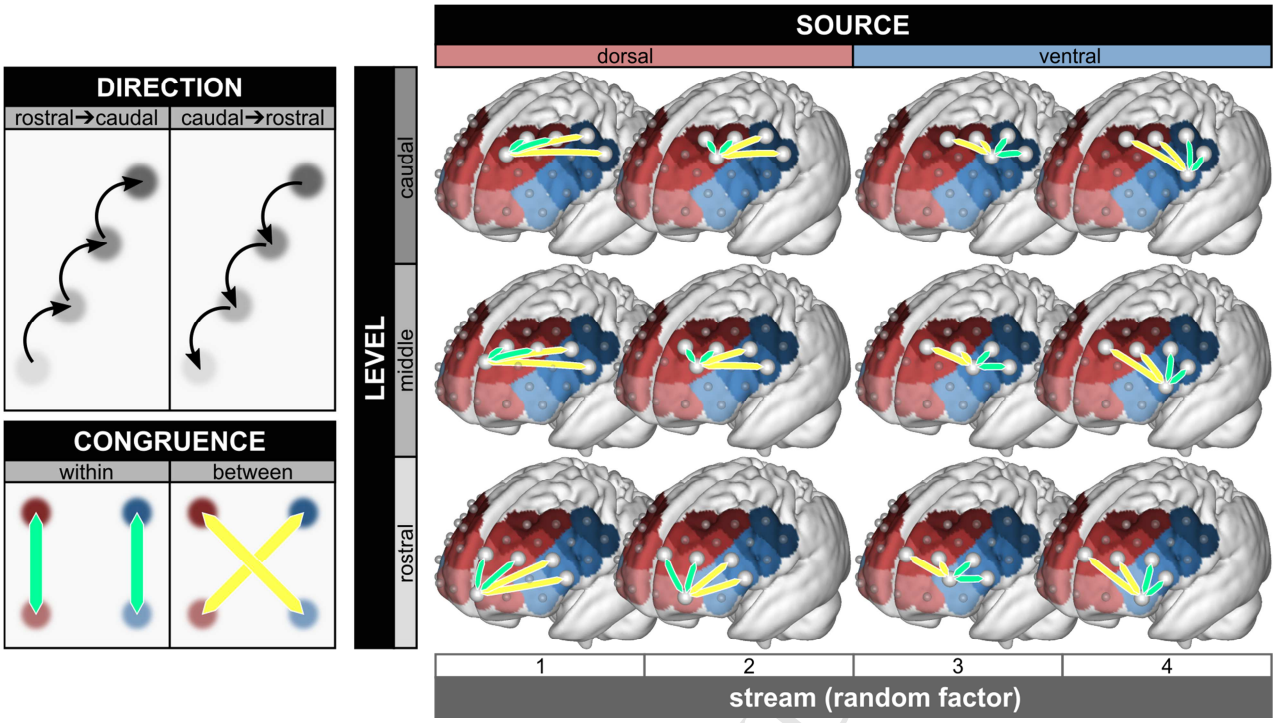

Figure 1, **Illustration of factors included in the linear mixed models and positions of fNIRS channels.** Selected connections for which DC values were analyzed in the mixed models are illustrated here for the left hemisphere but were identically applied in the right hemisphere. Hemisphere and stream (position of source channel along the ventro-dorsal axis) were included as random factors in the analyses. The **direction** of connections was classified as either rostral-to-caudal or as caudal-to-rostral. The factor **congruence** divided influences into those *within* the ventral and dorsal streams (green) and into those *between* the ventral and dorsal streams (yellow). The position of connections along the rostro-caudal axis (light to dark colors) was identified by the factor **level**. **Model #1** considered the factors **direction**, **congruence** and **level**. In **Model #2**, only directed interactions in rostral-to-caudal direction were considered, thereby eliminating the factor direction. Instead, factor **source** introduced the differentiation between influences originating from *ventral* (blue regions) and *dorsal* (red regions) PFC. Thus, in Model #2 factors **congruence** and **level** were analogous to Model #1, except that only rostro-caudally directed influences were included.

Results

Due to the high number of observations all fixed effects terms in both models were significant ($p < .05$); we therefore only report significant digits (Clymo, 2014) of least square means of DC values (DC_{LSM}) ± standard errors and post-hoc tests of interest in the text and refer the reader to Supplementary Table S1 for a detailed overview of effect statistics. In the following, ΔDC_{LSM} denotes contrasts (pairwise comparisons) of DC_{LSM} values and $\Delta\Delta DC_{LSM}$ denotes interaction contrast (pairwise comparisons of pairwise comparisons).

Rostro-caudally directed interactions dissociate into ventral and dorsal components (Model #1)

Directed interactions along the rostro-caudal axis in the PFC were assessed by means of directed coherence (DC) from and toward 16 reference channels (per hemisphere) placed on the ventral and dorsal convexity of the lateral PFC (Fig. 1). Model #1 comprised the fixed within-subject factors direction, congruence, and level and the main effect for direction revealed that caudally directed influences (DC_{LSM} = .417 ± .005) were significantly higher than those directed rostrally (DC_{LSM} = .286 ± .005; ΔDC_{LSM} = .131 ± .004, p < .0001). Regarding the main effect for level, influences at the middle level (DC_{LSM} = .370 ± .006) were significantly larger than at the rostral (DC_{LSM} = .341 ± .006; middle-rostral: ΔDC_{LSM} = .030 ± .005, p < .0001) and caudal level (DC_{LSM} = .344 ± .006; middle-caudal: ΔDC_{LSM} = .027 ± .005, p < .0001). There was no significant difference between the rostral and the caudal level (ΔDC_{LSM} = .003 ± .005, p = .85). The main effect for congruence further revealed that directed interactions between the ventral and the dorsal channel rows (DC_{LSM} = .338 ± .005) were lower than those within ventral and within dorsal rows (DC_{LSM} = .366 ± .005; ΔDC_{LSM} = .029 ± .004, p < .0001). The significant two-way interaction between level and direction indicated that the difference between the directions of influences varied across levels, i.e. across regions along the rostro-caudal axis. The corresponding pairwise comparisons showed that (i) on all levels, caudally directed influences were higher than rostrally directed influences (rostral: ΔDC_{LSM} = .050 ± .008, middle: ΔDC_{LSM} = .214 ± .008, caudal: ΔDC_{LSM} = .130 ± .008; all p < .0001) and (ii) that the difference between directions on the middle level was larger than on the rostral ($\Delta\Delta DC_{LSM}$ = .16 ± .01, p < .0001) and on the caudal ($\Delta\Delta DC_{LSM}$ = .08 ± .01, p < .0001) level, and larger on the caudal compared to the rostral level ($\Delta\Delta DC_{LSM}$ = .08 ± .01, p < .0001). Taken together the rostro-caudal gradient was strong in the mid-lateral PFC but only weak in the rostral PFC (Fig. 2).

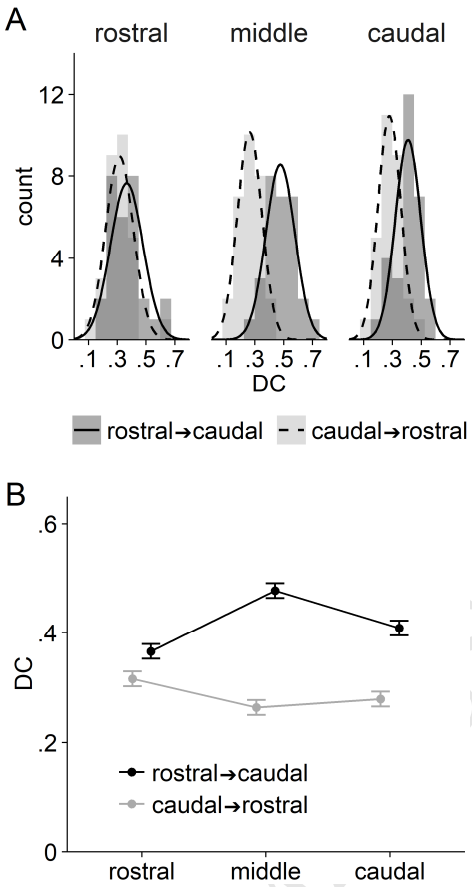

Figure 2: **Model #1. Two-way interaction between level and direction.** (A) Histogram of DC values aggregated across factors session, hemisphere, stream and congruence, i.e. each participant contributes one count to each histogram. Lines represent normal distributions fitted to the aggregated DC values. (B) Least square means with 95% confidence intervals. Both plots demonstrate a marked prevalence for rostro-caudally directed influences at the middle and caudal level, whereas there was little difference between directions at the rostral level.

Similar effects were established by the significant two-way interactions between direction and congruence: The rostro-caudal gradient (i.e. the difference between caudally and rostrally directed influences) was always positive, but greater within than between ventral and dorsal PFC (within: ΔDC_{LSM} = .143 ± .006, p < .0001; between: ΔDC_{LSM} = .119 ± .006, p < .0001; within vs. between: $\Delta\Delta DC_{LSM}$ = .024 ± .009, p = .009). Regarding the interaction between level and congruence, influences at the middle and caudal level were stronger within than between channel rows in ventral and dorsal PFC (middle: ΔDC_{LSM} = .040 ± .008, caudal: ΔDC_{LSM} = .040 ± .008, both p < .0001). At the rostral level, this difference was concordant, but not significant (ΔDC_{LSM} = .004 ± .008, p = .61). The contrast of congruence was significantly larger on the middle than on the rostral level ($\Delta\Delta DC_{LSM}$ = .04 ± .01, p = .003), larger on the caudal than on the rostral level ($\Delta\Delta DC_{LSM}$ = .04 ± .01, p = .003)

and equal on the middle and caudal level ($\Delta\Delta DC_{LSM}$ = .00 ± .01, p > .99). Finally, the significant three-way interaction between direction, congruence, and level revealed that (i) for the rostral-to-caudal direction, again only at the middle and caudal level, influences within ventral and dorsal were significantly stronger than between ventral and dorsal PFC (rostral: ΔDC_{LSM} = .00 ± .01, p = .88; middle: ΔDC_{LSM} = .07 ± .01, caudal: ΔDC_{LSM} = .05 ± .01, both p < .0001, Fig. 3 left panels), whereas (ii) for the caudal-to-rostral direction, this was only the case at the caudal level (rostral: ΔDC_{LSM} = .01 ± .01, p = .38; middle: ΔDC_{LSM} = .01 ± .01, p = .22; caudal: ΔDC_{LSM} = .03 ± .01, p = .02, Fig. 3 right panels). Taken together, for the predominant rostral-to-caudal direction, the segregation between ventral and dorsal PFC was apparent only on the middle and caudal level. In contrast, for the weaker caudo-rostrally directed influences the ventro-dorsal segregation was evident only on the caudal level (Fig. 3).

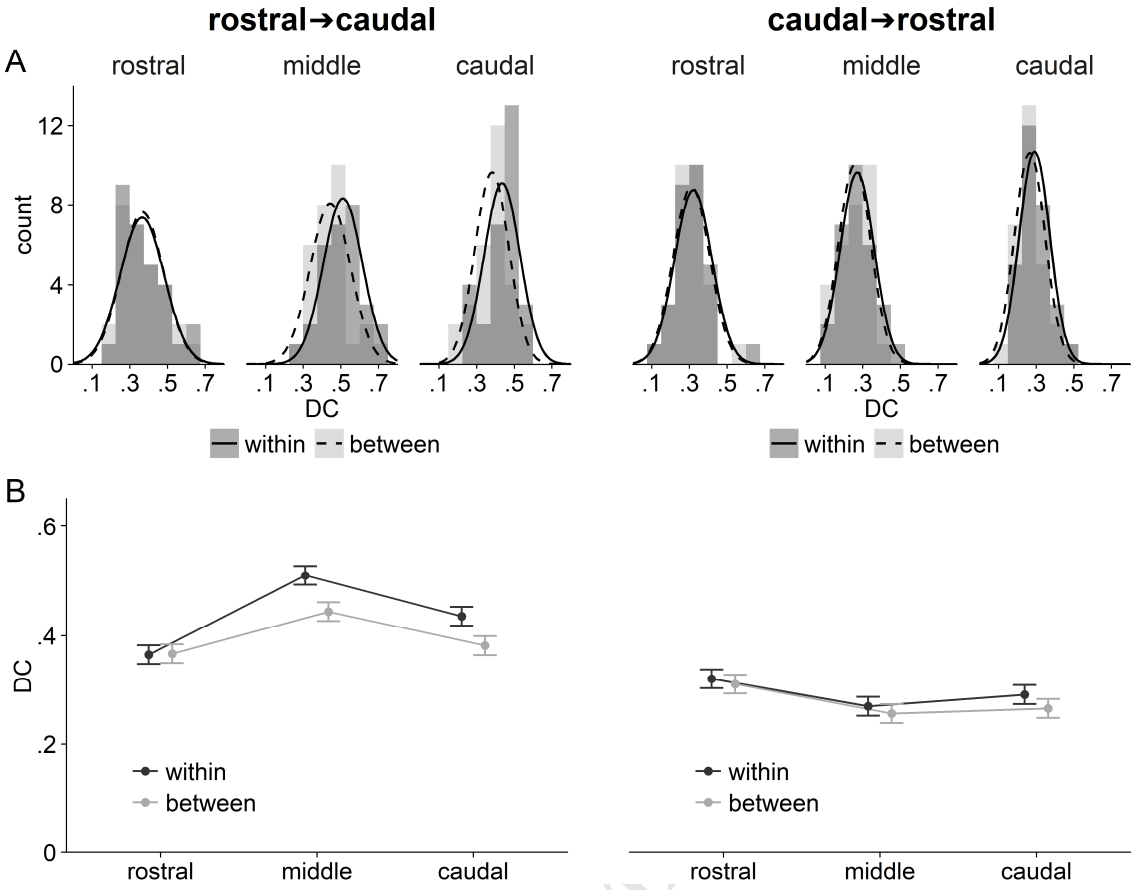

Figure 3: **Model #1. Three-way interaction between level, congruence and direction.** (A) Histogram of DC values aggregated across the random factors session, hemisphere and stream, i.e. each participant contributes one count to each histogram. Lines represent normal distributions fitted to the aggregated DC values. (B) Least square means with 95% confidence intervals. For rostro-caudally directed influences (left panels), DC revealed higher influences within, than between dorsal and ventral PFC at the middle and caudal level, while there was no difference at the rostral level. In contrast, for the caudal-to-rostral direction (right panels), the caudal level was the only one showing a small, but significant difference when comparing influences within vs. between ventral and dorsal PFC.

The main results from Model #1 for the 16 selected channels (Fig. 1) were also reflected by the renderings of the directed influences across all 38 prefrontal channels (Fig. 4): Influences between PFC regions as measured by DC revealed higher influences *from rostral references* toward caudal areas than *from caudal references* toward rostral areas (Fig. 4A). Complementarily, influences *toward rostral references* from caudal areas were inferior to those *toward caudal references* from rostral areas (Fig. 4B). These relations were observed irrespective of whether the reference channel was on the dorsal (Fig. 4 outer columns) or on the ventral convexity (Fig. 4 middle two columns). The net-influences in terms of the difference between the directions of influences, projected on the cortical surface are illustrated in Supplementary Figure S4.

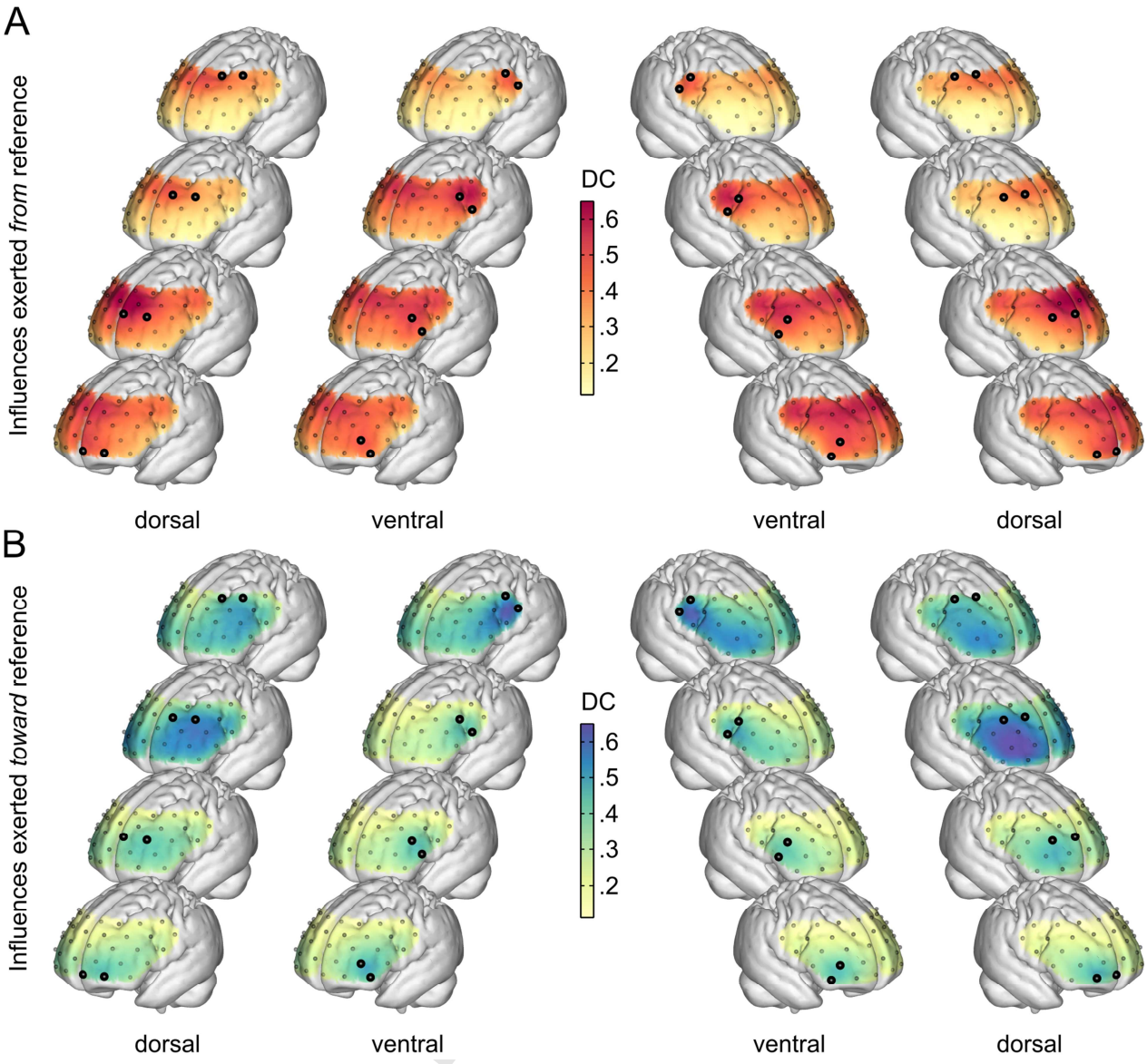

298 Figure 4: **Influences from (A) and toward (B) reference channels** as measured by DC, averaged over both testing sessions
299 and all subjects. Reference channels are marked black; each brain represents the average over two reference channels. Hot
300 and cold colors indicate high influences from and toward reference channels, respectively. (A) Influences *from references* on
301 regions rostral to the references were *lower* than on regions caudal to the references. (B) Conversely, influences *toward*
302 *references* originating in regions rostral to the references were *higher* than in regions caudal to the references. The contrast
303 between the influences plotted in panels A and B, i.e. the net-influences of each reference channel, reflecting the rostro-
304 caudal asymmetry of influences is provided in Supplementary Figure S4.

305 **Interactions between the ventral and dorsal stream (Model #2)**

306 Model #2 was designed to assess differences between influences exerted by ventral and dorsal
307 reference channels, regarding only the predominant rostral-to-caudal direction. The linear mixed
308 model comprised the within-subject factors source, congruence, and level (Fig. 1). For the main effect
309 of source, influences from ventral channels (DC_{LSM} = .456 ± .008) were stronger than from dorsal

channels (DC_{LSM} = .379 ± .008; ΔDC_{LSM} = .08 ± .01, p < .0001). The main effect of congruence again showed that directed interactions within ventral and dorsal channel rows (DC_{LSM} = .437 ± .006) exceeded those between rows (DC_{LSM} = .397 ± .006; ΔDC_{LSM} = .040 ± .007, p < .0001). The main effect of level revealed directed interactions at the rostral level (DC_{LSM} = .366 ± .007) to be lower than at the middle (DC_{LSM} = .477 ± .007; ΔDC_{LSM} = .111 ± .008, p < .0001) and caudal level (DC_{LSM} = .409 ± .007; ΔDC_{LSM} = .043 ± .008, p < .0001). Directed interactions at the middle level were stronger than at the caudal level (ΔDC_{LSM} = .069 ± .008, p < .0001). A significant two-way interaction between level and congruence again indicated that directed interactions were higher within than between ventral and dorsal PFC only at the middle (ΔDC_{LSM} = .07 ± .01, p < .0001) and caudal level (ΔDC_{LSM} = .05 ± .01, p < .0001) and equal in the rostral PFC (ΔDC_{LSM} = .00 ± .01, p = .88). Likewise, a significant two-way interaction between level and source further showed that the predominance of directed interactions originating from ventral channels compared to influences from dorsal channels increased from rostral to caudal PFC (rostral: ΔDC_{LSM} = .03 ± .01, p = .03; middle: ΔDC_{LSM} = .03 ± .01, p = .02; caudal: ΔDC_{LSM} = .17 ± .01, p < .0001; Fig. 5). A significant two-way interaction between source and congruence yielded that directed interactions from dorsal toward other dorsal channels were higher than toward ventral channels (ΔDC_{LSM} = .125 ± .009, p < .001). In contrast, directed interactions within ventral channel rows were lower than from ventral toward dorsal PFC (ΔDC_{LSM} = .045 ± .009, p < .001). However, a significant three-way interaction revealed a disordinal relationship between level and congruence for the ventral sources (Fig. 5, right panels): At the rostral and middle level, directed interactions from ventral toward dorsal PFC were stronger than within ventral PFC (rostral: ΔDC_{LSM} = .09 ± .02, p < .0001; middle: ΔDC_{LSM} = .14 ± .02, p < .0001), while at the caudal level interactions within ventral PFC were stronger than from ventral toward dorsal PFC (ΔDC_{LSM} = .09 ± .02, p < .0001).For the dorsal sources (Fig. 5, left panels), directed interactions at the rostral and caudal levels were stronger on other dorsal channels than on ventral channels (rostral: ΔDC_{LSM} = .09 ± .02, p < .0001; middle: ΔDC_{LSM} = .27 ± .02, p < .0001), but there was no significant difference on the caudal level (ΔDC_{LSM} = .02 ± .02, p = .28). In summary, the most pronounced rostro-caudal influences were exerted within the mid-dorsolateral PFC, from mid-ventrolateral toward mid-dorsolateral and within caudo-ventral regions.

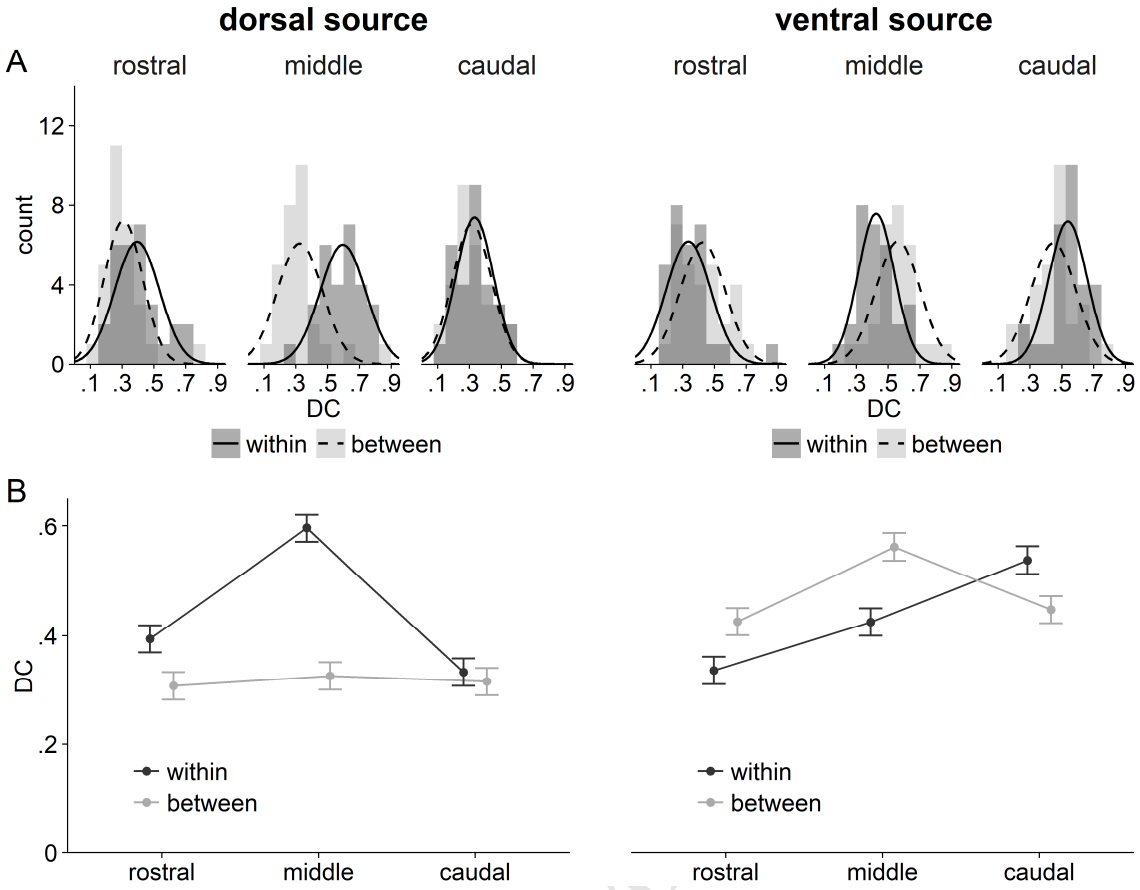

Figure 5: **Model #2. Three-way interaction between level, congruence and source.** (A) Histogram of DC values for rostro-caudally directed influences aggregated across session, hemisphere and streams within ventral and dorsal PFC, i.e. each participant contributes one count to each histogram. Lines represent normal distributions fitted to the aggregated DC values. (B) Least square means with 95% confidence intervals. For dorsal sources (left panels), influences directed caudally were always stronger toward other dorsal channels than toward ventral channels. This dissociation is most pronounced for the middle level and was not significant at the caudal level. Influences exerted by ventral sources (right panels) increased from rostral to caudal PFC. At the rostral and middle level the influence from ventral to dorsal exceeded the influence within the ventral channels, whereas influences within ventral PFC predominated at the caudal-most level.

Long-distance connections

To facilitate a balanced factorial design, Model #1 and #2 considered only connections between adjacent channels, i.e. only a subset of all possible channel pairs. In order to extend the scope of the present analyses, Supplementary Model #3 included connections between distant channel pairs and assessed the rostro-caudal and ventro-dorsal influences across long-range connections. Results of Supplementary Model #3 were generally in line with Model #1 and #2 but additionally revealed that (i) the rostro-caudal asymmetry of influences increased with the length of connections with the rostral-most region exerting strong influences on caudal PFC (and not vice versa) and (ii) that the segregation into the ventral and dorsal component was only existent for short connections between rostro-caudally

adjacent channels and not for long-range connections. For further details see Supplementary Analysis (Model #3) and Supplementary Figures S5 – S7.

Exhaustive vector representation of influences within and between dorsal and ventral PFC

Mixed models #1 - #3 tested hypotheses about influences of specific directions. However, the spatial representation of connections as vectors allows a more comprehensive illustration of influences between PFC regions. Figure 6 therefore shows all within-hemisphere connections as vectors superposed on the cortical surface (see also Supplementary Figure S8 for a full connectivity matrix). At each channel position, all influences from (Fig. 6A) and toward (Fig. 6B) that channel are represented as lines pointing toward the respective 2nd channel with the length of the line defined by the DC value (i.e. representing the strength of the influence). Averages across connections of each channel and across connections of all ventral and all dorsal channels are shown as arrows with black and white outlines respectively. The vector representation reflects the results of the mixed model analyses as for within-connections, rostral channels were stronger causal sources than caudal channels (Fig. 6 A, left) and caudal channels were stronger causal sinks than rostral channels (Fig. 6 B, left). For between-connections, ventral channels were stronger sources than dorsal channels (Fig. 6 A, right) and dorsal channels were stronger sinks than ventral channels (Fig. 6 B, right). The length of arrows representing average within- and average between-influences suggest that – contrary to the results of Model #1 – influences were stronger between than within ventral and dorsal PFC. However, it is essential to recognize that the arrangement of channels biased the length of the average vectors. Specifically, the length of between-vectors (right) tend to sum-up as they all point in a similar direction, while for within-vectors (left) lengths tend to average out. The vector representation of the net-influences in terms of the difference between influences exerted by and on channels is shown in Supplementary Figure S9.

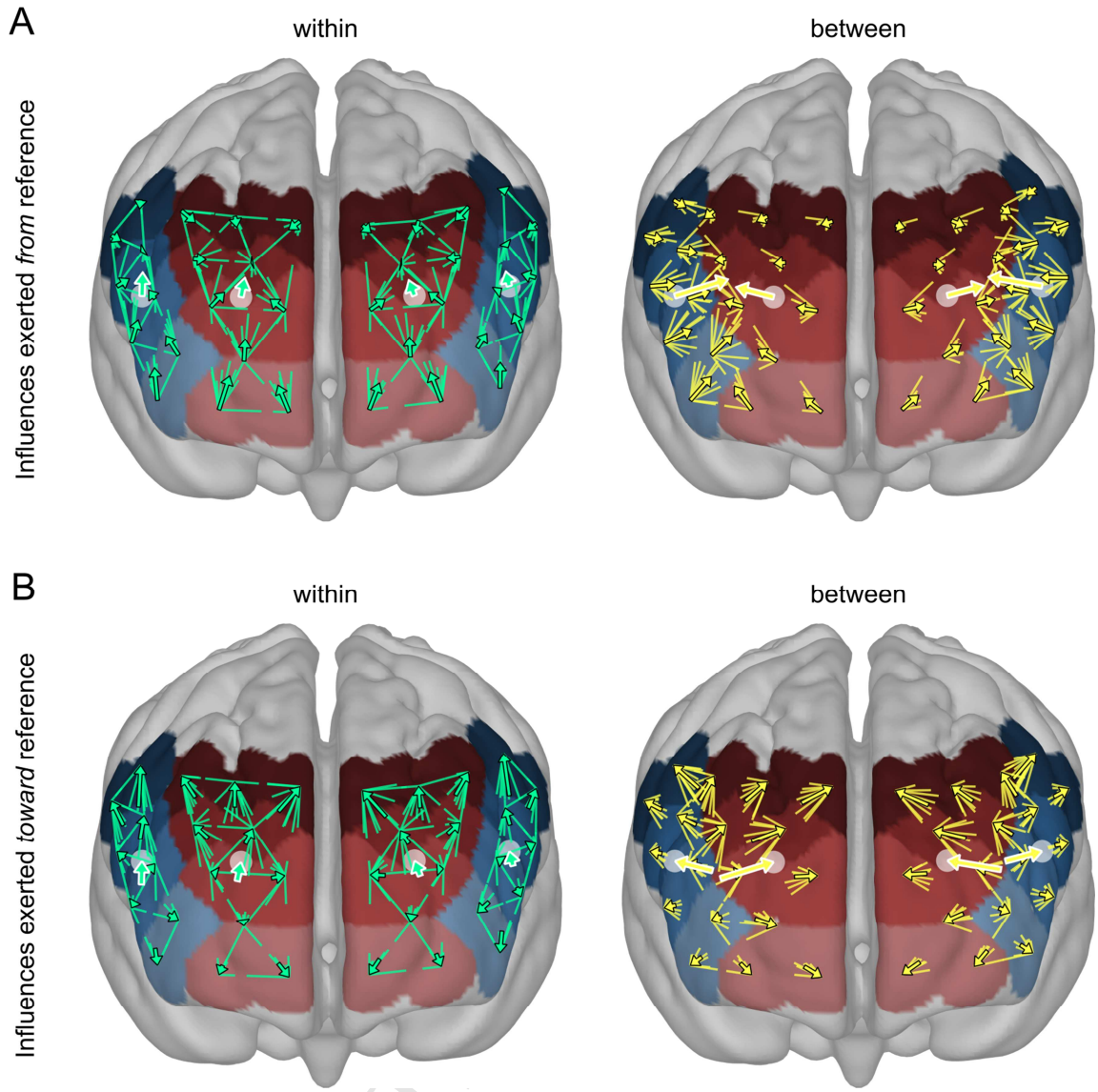

Figure 6: **Vector representation of influences within and between ventral and dorsal PFC**. Within each hemisphere, all connections within (green vectors, left) and between (yellow vectors, right) ventral (blue surface) and dorsal (red surface) channel pairs are represented by vectors. The illustration reflects results of the mixed model analyses as (i) rostral channels exerted stronger influences than caudal channels (A), (ii) caudal channels received stronger influences than rostral channels (B) and (iii) influences from ventral toward dorsal PFC were stronger than vice versa (A and B, right brains). (A) At the position P_i of channel i the influence i→j is represented as a line of length $DC_{i\rightarrow j}$ pointing toward channel j. (B) At the position P_i of channel i the influence i←j is represented as a line of length $DC_{i\leftarrow j}$ pointing toward channel j. At each position the average of vectors is indicated by arrows. Big arrows with white outlines represent averages for ventral and dorsal channels at the mean position of the respective channels (indicated as white circles). Vectors were calculated in two dimensions (in the x-z-plane after rotation around the x-axis by 15 degrees) and were superposed on the cortical surface for spatial assignment. Note that the length of mean vectors for within-connections and between-connections shown as arrows are not comparable, because for between-connections (right) the length of vectors tend to sum-up as they all point in a similar direction, while for within-connections (left) directionality of vectors tend to average out; thus, direction and length of mean vectors are biased by the arrangement of channels.

Discussion

Taking advantage of the sufficiently high temporal and spatial resolution of multi-channel fNIRS, the present study used directed coherence as a measure of influences between brain regions to assess the functional networks of the PFC (Medvedev, 2014). Showing that activity in caudal PFC is modulated by activity in its more rostral parts, the present data provide complementary evidence for the intrinsic rostro-caudal functional hierarchy within the PFC, as predicted by extant models of prefrontal organization (Badre and Nee, 2018). More specifically, the rostro-caudal asymmetry of influences is most pronounced in the mid-lateral PFC, but only marginal in its rostral-most part. Furthermore, this effect is segregated into a ventral and a dorsal component.

The rostro-caudally directed hierarchy of neural processing in the PFC

Confirming previous assumptions (Badre and D'Esposito, 2009; Koechlin et al., 2003), Model #1 revealed a predominance of rostro-caudally directed influences. However, this pattern was not uniformly evident across the rostro-caudal axis, as directed interactions on the rostral-most level appeared to be almost balanced between both directions (Fig. 2). First of all, this finding does not contradict the general validity of the rostro-caudal hierarchy hypothesis, because the overall influences from the rostral channels *on the rest of the PFC* (Fig. 4A) exceeded by far the influences toward the rostral channels *from the rest of the PFC* (Fig. 4B), i.e. the rostro-caudal gradient was evident especially for long connections (also see Supplementary Analysis). Second, recent findings indicate that mid-lateral PFC and not rostral PFC may represent the apex of the hierarchical processing in the PFC (Badre and Nee, 2018; Margulies et al., 2016; Nee and D'Esposito, 2016) thus suggesting increased caudo-rostrally directed interactions between mid-lateral and rostral PFC. In line with this, influences from rostral to mid-lateral PFC were only marginally stronger than vice versa.

Yet, the rostral PFC is often associated with the representation of the most abstract rules and the selection of goal-relevant information which should be processed within the apex of the hierarchy (Badre and D'Esposito, 2009, 2007). As such task demands were not externally triggered in the present study, the intrinsic activation level might have been too low to reveal directed interactions on this small spatial scale. In turn, the influences over a longer distance, however, might have

accumulated over the intermediate stages of the rostro-caudal hierarchy. That is, information, as it is propagated from rostral to caudal PFC, might be enriched by intermediate nodes and accumulate on lower levels of the rostro-caudal hierarchy (Koechlin et al., 2003; Koechlin and Summerfield, 2007). The basic idea of this accumulation hypothesis is that superordinate information on higher levels needs to be maintained over time, because it guides sequences of information selection processes on lower levels, which are relevant in a more confined context only (Koechlin et al., 2003; Koechlin and Summerfield, 2007). In other words, more rostral regions maintain persistent information, whereas more caudal regions process transient information with higher throughput. In line with this, caudally directed influences on the rostral level were lower than on the middle and caudal level (Fig. 2) and the rostro-caudal asymmetry of directed interactions between more distant regions was higher than between adjacent regions (see Supplementary Materials for an analysis of long-distance connections and Supplementary Figure S6). Thus, if neural activity propagates from rostral to caudal PFC, the amount of transferred information may increase toward caudal regions, as the information is substantiated on the intermediate processing stages. In sum, the present results argue for the implementation of cognitive control by a prefrontal rostro-caudal processing hierarchy that peaks in mid-lateral PFC rather than in the frontopolar cortex (cf. Badre and Nee, 2018). However, results also support a hierarchical relationship between frontopolar and caudal PFC with rostro-caudal connections bypassing mid-lateral PFC. Thus, the PFC network may constitute a concentric network topology with the mid-lateral PFC as the main hub and the frontopolar cortex as a complementary downstream route to caudal PFC.

Ventral and dorsal components of the rostro-caudal gradient in the PFC

Model #1 showed that connectivity within dorsal and ventral PFC was stronger than the connectivity between the two regions and, furthermore, that this difference was directionally and regionally specific (Fig. 3). This segregation is also reflected by findings concerning differences between ventral and dorsal PFC in their ontogenetic development (Gogtay et al., 2004), in their cytoarchitecture (Petrides and Pandya, 2002, 1999), in their structural connectivity with posterior cortex (Saur et al., 2008; Takahashi et al., 2013), and in their association with different executive functions (Bahlmann et al., 2012; D'Esposito et al., 1999; Owen, 1997) and even by differential behavioral outcome after

optogenetic inhibition of PFC subregions in the rat (Hardung et al., 2017). However, while there exist many studies on the segregation of these two regions (e.g. Bahlmann et al. (2015), Blumenfeld, Lee, & D'Esposito (2014), Swann, Tandon, Pieters, & Aron (2013); for reviews see Blumenfeld & Ranganath (2007), Tanji & Hoshi (2008)), considerably less attention has been paid on how they may interact. In this regard, ventral PFC has been shown to be associated with the retrieval, selection, and maintenance of goal-relevant information (Badre et al., 2005; Bunge et al., 2004; D'Esposito et al., 1999; Thompson-Schill et al., 1997), whereas the dorsal part is additionally recruited for the manipulation and monitoring of goal-relevant information (Bunge et al., 2003; Christoff et al., 2001; D'Esposito et al., 1999; Garavan et al., 2000). In Model #2 the rostro-caudally directed interactions from ventral and dorsal PFC were considered separately (Fig. 5) revealing asymmetric influences between these two parts of the PFC. It hence seems that the dorsal and ventral components of the rostro-caudal hierarchy are segregated, but not coequal. More specifically, influences from ventral toward dorsal PFC were consistently stronger than from dorsal toward ventral PFC.

If retrieval and selection of information from memory or sensory association cortices is accomplished by the ventral PFC and manipulation of this information by the dorsal PFC (Bunge et al., 2004; Race et al., 2009), a bottom-up pathway from ventral to dorsal PFC seems obvious in that the external information is introduced by ventral PFC for manipulation in dorsal areas. Yet, the selection process within the ventral PFC is unlikely to be autonomous, but probably supported by top-down feedback from dorsal PFC (Swann et al., 2013) or gated by the basal ganglia (Badre and Frank, 2012; Hazy et al., 2007). Therefore, hierarchical processing in ventral PFC might provide a filter for external inputs, which serve hierarchical processing in dorsal PFC with currently relevant information to be involved in the evaluation of goal directed behavior by the dorsal processing hierarchy. Thus, from these assumptions it follows that directed interactions between dorsal and ventral PFC should be modulated by task demands that require the selection of specific stimuli according to a current task rule. Given that the present recordings comprised neural activity in a task-free state, these predictions remain to be tested in future studies.

Finally, on the rostral-most level in Model #1 we did not find a predominant direction of rostro-caudal interactions, but when examining influences from ventral and dorsal rostral PFC separately in Model #2, it was revealed that rostral references exerted stronger influences toward dorsal than ventral PFC. This seems to contradict the hypothesis that the segregation of ventral and dorsal regions would be more pronounced than their interaction. However, the rostral-most reference channels probably sampled a part of the lateral Brodmann area 10, which co-activates with a wide variety of other prefrontal regions in very different task paradigms (Gilbert et al., 2010). It has been proposed that area 10 fulfills a supervisory function and helps to guide attention to currently relevant information (Bunge et al., 2005, 2003; Burgess et al., 2007). As such, it might constitute a monitoring entity that evaluates current abstract goals represented by rostral levels and revises ongoing action selection processed by caudal levels of the hierarchy. In this scenario, area 10 would not be integrated in the rostro-caudal hierarchy but differentially interact with each hierarchical level to regulate the parallel ventral and dorsal information cascades. This interpretation is also supported by the spatial illustration of influences in Figure 4 and the supplementary analysis considering long-range connections from rostral to caudal PFC (Model #3), which on the one hand revealed strong influences exerted by the rostral-most on the caudal-most level (Supplementary Figure S6), and on the other hand showed that these long-range connections did *not* separate into a ventral and a dorsal component (Supplementary Figure S7).

Conclusion

Using the methodological framework of fast sampling multi-channel fNIRS and a frequency-domain measure of directed functional connectivity, we provide explicit evidence for a rostral-to-caudal processing hierarchy in the PFC. Consistent with extant models of prefrontal organization, this hierarchy is dissociated into a ventral and a dorsal component and peaks in the mid-dorsolateral PFC, which exerts the highest level of cognitive control (Badre and Nee, 2018).

References

Ashburner, J., 2007. A fast diffeomorphic image registration algorithm. Neuroimage 38, 95–113. https://doi.org/10.1016/j.neuroimage.2007.07.007

Azuar, C., Reyes, P., Slachevsky, A., Volle, E., Kinkingnehun, S., Kouneiher, F., Bravo, E., Dubois, B., Koechlin, E., Levy, R., 2014. Testing the model of caudo-rostral organization of cognitive control in the human with frontal lesions. Neuroimage 84, 1053–60. https://doi.org/10.1016/j.neuroimage.2013.09.031

Badre, D., D'Esposito, M., 2009. Is the rostro-caudal axis of the frontal lobe hierarchical? Nat. Rev. Neurosci. 10, 659–69. https://doi.org/10.1038/nrn2667

Badre, D., D'Esposito, M., 2007. Functional magnetic resonance imaging evidence for a hierarchical organization of the prefrontal cortex. J. Cogn. Neurosci. 19, 2082–2099.

Badre, D., Frank, M.J., 2012. Mechanisms of hierarchical reinforcement learning in cortico-striatal circuits 2: Evidence from fMRI. Cereb. Cortex 22, 527–536. https://doi.org/10.1093/cercor/bhr117

Badre, D., Hoffman, J., Cooney, J.W., D'Esposito, M., 2009. Hierarchical cognitive control deficits following damage to the human frontal lobe. Nat. Neurosci. 12, 515–22. https://doi.org/10.1038/nn.2277

Badre, D., Nee, D.E., 2018. Frontal Cortex and the Hierarchical Control of Behavior. Trends Cogn. Sci. 22, 170–188. https://doi.org/10.1016/j.tics.2017.11.005

Badre, D., Poldrack, R.A., Paré-Blagoev, E.J., Insler, R.Z., Wagner, A.D., 2005. Dissociable controlled retrieval and generalized selection mechanisms in ventrolateral prefrontal cortex. Neuron 47, 907–18. https://doi.org/10.1016/j.neuron.2005.07.023

Bahlmann, J., Blumenfeld, R.S., D'Esposito, M., 2015. The Rostro-Caudal Axis of Frontal Cortex Is Sensitive to the Domain of Stimulus Information. Cereb. Cortex 25, 1815–26. https://doi.org/10.1093/cercor/bht419

523 Bahlmann, J., Korb, F.M., Gratton, C., Friederici, A.D., 2012. Levels of integration in cognitive
524 control and sequence processing in the prefrontal cortex. PLoS One 7, e43774.
525 https://doi.org/10.1371/journal.pone.0043774

526 Bartels, A., Zeki, S., 2005. Brain dynamics during natural viewing conditions--a new guide for
527 mapping connectivity in vivo. Neuroimage 24, 339–49.
528 https://doi.org/10.1016/j.neuroimage.2004.08.044

529 Bates, D., Mächler, M., Bolker, B., Walker, S., 2015. Fitting Linear Mixed-Effects Models Using
530 lme4. J. Stat. Softw. 67, 1–48. https://doi.org/10.18637/jss.v067.i01

531 Beck, A.T., Steer, R.A., Brown, G.K., 1996. Manual for the Beck Depression Inventory–II. The
532 Psychological Corporation, Harcourt Brace, San Antonio, TX.

533 Biswal, B., Yetkin, F.Z., Haughton, V.M., Hyde, J.S., 1995. Functional connectivity in the motor
534 cortex of resting human brain using echo-planar MRI. Magn. Reson. Med. 34, 537–41.
535 https://doi.org/10.1002/mrm.1910340409

536 Blumenfeld, R.S., Bliss, D.P., D'Esposito, M., 2018. Quantitative Anatomical Evidence for a
537 Dorsoventral and Rostrocaudal Segregation within the Nonhuman Primate Frontal Cortex. J.
538 Cogn. Neurosci. 30, 353–364. https://doi.org/10.1162/jocn_a_01203

539 Blumenfeld, R.S., Lee, T.G., D'Esposito, M., 2014. The effects of lateral prefrontal transcranial
540 magnetic stimulation on item memory encoding. Neuropsychologia 53, 197–202.
541 https://doi.org/10.1016/j.neuropsychologia.2013.11.021

542 Blumenfeld, R.S., Nomura, E.M., Gratton, C., D'Esposito, M., 2013. Lateral prefrontal cortex is
543 organized into parallel dorsal and ventral streams along the rostro-caudal axis. Cereb. Cortex 23,
544 2457–66. https://doi.org/10.1093/cercor/bhs223

545 Blumenfeld, R.S., Ranganath, C., 2007. Prefrontal cortex and long-term memory encoding: an
546 integrative review of findings from neuropsychology and neuroimaging. Neuroscientist 13, 280–
547 91. https://doi.org/10.1177/1073858407299290

548 Bunge, S.A., Burrows, B., Wagner, A.D., 2004. Prefrontal and hippocampal contributions to visual
549 associative recognition: interactions between cognitive control and episodic retrieval. Brain
550 Cogn. 56, 141–52. https://doi.org/10.1016/j.bandc.2003.08.001

551 Bunge, S.A., Kahn, I., Wallis, J.D., Miller, E.K., Wagner, A.D., 2003. Neural circuits subserving the
552 retrieval and maintenance of abstract rules. J. Neurophysiol. 90, 3419–28.
553 https://doi.org/10.1152/jn.00910.2002

554 Bunge, S.A., Wendelken, C., Badre, D., Wagner, A.D., 2005. Analogical reasoning and prefrontal
555 cortex: evidence for separable retrieval and integration mechanisms. Cereb. Cortex 15, 239–49.
556 https://doi.org/10.1093/cercor/bhh126

557 Burgess, P.W., Dumontheil, I., Gilbert, S.J., 2007. The gateway hypothesis of rostral prefrontal cortex
558 (area 10) function. Trends Cogn. Sci. 11, 290–298. https://doi.org/10.1016/j.tics.2007.05.004

559 Christoff, K., Prabhakaran, V., Dorfman, J., Zhao, Z., Kroger, J.K., Holyoak, K.J., Gabrieli, J.D.E.,
560 2001. Rostrolateral prefrontal cortex involvement in relational integration during reasoning.
561 Neuroimage 14, 1136–49. https://doi.org/10.1006/nimg.2001.0922

562 Clymo, R.S., 2014. Managing error, in: Reporting Research. Cambridge University Press, Cambridge,
563 pp. 211–242. https://doi.org/10.1017/CBO9781107284234.011

564 Cope, M., Delpy, D.T., 1988. System for long-term measurement of cerebral blood and tissue
565 oxygenation on newborn infants by near infra-red transillumination. Med. Biol. Eng. Comput.
566 26, 289–294. https://doi.org/10.1007/BF02447083

567 Crittenden, B.M., Duncan, J., 2014. Task difficulty manipulation reveals multiple demand activity but
568 no frontal lobe hierarchy. Cereb. Cortex 24, 532–40. https://doi.org/10.1093/cercor/bhs333

569 Cui, X., Bray, S., Reiss, A.L., 2010. Functional near infrared spectroscopy (NIRS) signal improvement
570 based on negative correlation between oxygenated and deoxygenated hemoglobin dynamics.
571 Neuroimage 49, 3039–46. https://doi.org/10.1016/j.neuroimage.2009.11.050

572 D'Esposito, M., Postle, B.R., Ballard, D., Lease, J., 1999. Maintenance versus manipulation of

information held in working memory: an event-related fMRI study. Brain Cogn. 41, 66–86. https://doi.org/10.1006/brcg.1999.1096

Florin, E., Gross, J., Pfeifer, J., Fink, G.R., Timmermann, L., 2010. The effect of filtering on Granger causality based multivariate causality measures. Neuroimage 50, 577–588. https://doi.org/http://dx.doi.org/10.1016/j.neuroimage.2009.12.050

Fothergill, A., Linfield, M., 2007. Earth. Universum Film GmbH, UK, Germany, USA.

Garavan, H., Ross, T.J., Li, S.-J., Stein, E.A., 2000. A parametric manipulation of central executive functioning. Cereb. Cortex 10, 585–592. https://doi.org/10.1093/cercor/10.6.585

Gilbert, S.J., Gonen-Yaacovi, G., Benoit, R.G., Volle, E., Burgess, P.W., 2010. Distinct functional connectivity associated with lateral versus medial rostral prefrontal cortex: A meta-analysis. Neuroimage 53, 1359–1367. https://doi.org/10.1016/j.neuroimage.2010.07.032

Gogtay, N., Giedd, J.N., Lusk, L., Hayashi, K.M., Greenstein, D., Vaituzis, a C., Nugent, T.F., Herman, D.H., Clasen, L.S., Toga, A.W., Rapoport, J.L., Thompson, P.M., 2004. Dynamic mapping of human cortical development during childhood through early adulthood. Proc. Natl. Acad. Sci. U. S. A. 101, 8174–9. https://doi.org/10.1073/pnas.0402680101

Goulas, A., Uylings, H.B.M., Stiers, P., 2014. Mapping the Hierarchical Layout of the Structural Network of the Macaque Prefrontal Cortex. Cereb. Cortex 24, 1178–1194. https://doi.org/10.1093/cercor/bhs399

Granger, C.W.J., 1969. Investigating Causal Relations by Econometric Models and Cross-spectral Methods. Econometrica 37, 424. https://doi.org/10.2307/1912791

Hardung, S., Epple, R., Jäckel, Z., Eriksson, D., Uran, C., Senn, V., Gibor, L., Yizhar, O., Diester, I., 2017. A Functional Gradient in the Rodent Prefrontal Cortex Supports Behavioral Inhibition. Curr. Biol. 27, 549–555. https://doi.org/10.1016/j.cub.2016.12.052

Hazy, T.E., Frank, M.J., O'reilly, R.C., 2007. Towards an executive without a homunculus: computational models of the prefrontal cortex/basal ganglia system. Philos. Trans. R. Soc. Lond.

598 B. Biol. Sci. 362, 1601–13. https://doi.org/10.1098/rstb.2007.2055

599 Koechlin, E., Basso, G., Pietrini, P., Panzer, S., Grafman, J., 1999. The role of the anterior prefrontal
600 cortex in human cognition. Nature 399, 148–51. https://doi.org/10.1038/20178

601 Koechlin, E., Ody, C., Kouneiher, F., 2003. The architecture of cognitive control in the human
602 prefrontal cortex. Science 302, 1181–5. https://doi.org/10.1126/science.1088545

603 Koechlin, E., Summerfield, C., 2007. An information theoretical approach to prefrontal executive
604 function. Trends Cogn. Sci. 11, 229–35. https://doi.org/10.1016/j.tics.2007.04.005

605 Köstering, L., Nitschke, K., Schumacher, F.K., Weiller, C., Kaller, C.P., 2015. Test-retest reliability of
606 the Tower of London Planning Task (TOL-F). Psychol. Assess. 27, 925–31.
607 https://doi.org/10.1037/pas0000097

608 Kuznetsova, A., Bruun Brockhoff, P., Haubo Bojesen Christensen, R., 2016. lmerTest: Tests in Linear
609 Mixed Effects Models.

610 Lenth, R. V, 2016. Least-Squares Means: The R Package lsmeans. J. Stat. Softw. 69, 1–33.
611 https://doi.org/10.18637/jss.v069.i01

612 Logothetis, N.K., 2008. What we can do and what we cannot do with fMRI. Nature 453, 869–78.
613 https://doi.org/10.1038/nature06976

614 Lowe, M.J., Dzemidzic, M., Lurito, J.T., Mathews, V.P., Phillips, M.D., 2000. Correlations in low-
615 frequency BOLD fluctuations reflect cortico-cortical connections. Neuroimage 12, 582–7.
616 https://doi.org/10.1006/nimg.2000.0654

617 Mader, W., Feess, D., Lange, R., Saur, D., Glauche, V., Weiller, C., Timmer, J., Schelter, B., 2008. On
618 the Detection of Direct Directed Information Flow in fMRI. IEEE J. Sel. Top. Signal Process. 2,
619 965–974. https://doi.org/10.1109/JSTSP.2008.2008260

620 Mansouri, F.A., Koechlin, E., Rosa, M.G.P., Buckley, M.J., 2017. Managing competing goals — a key
621 role for the frontopolar cortex. Nat. Rev. Neurosci. 18, 645–657.

https://doi.org/10.1038/nrn.2017.111

Margulies, D.S., Ghosh, S.S., Goulas, A., Falkiewicz, M., Huntenburg, J.M., Langs, G., Bezgin, G., Eickhoff, S.B., Castellanos, F.X., Petrides, M., Jefferies, E., Smallwood, J., 2016. Situating the default-mode network along a principal gradient of macroscale cortical organization. Proc. Natl. Acad. Sci. U. S. A. 113, 12574–12579. https://doi.org/10.1073/pnas.1608282113

Medvedev, A. V., 2014. Does the resting state connectivity have hemispheric asymmetry? A near-infrared spectroscopy study. Neuroimage 85, 400–407. https://doi.org/10.1016/j.neuroimage.2013.05.092

Nee, D.E., D'Esposito, M., 2017. Causal evidence for lateral prefrontal cortex dynamics supporting cognitive control. Elife 6, e28040. https://doi.org/10.7554/eLife.28040

Nee, D.E., D'Esposito, M., 2016. The hierarchical organization of the lateral prefrontal cortex. Elife 5, 1–26. https://doi.org/10.7554/eLife.12112

Owen, A.M., 1997. The functional organization of working memory processes within human lateral frontal cortex: the contribution of functional neuroimaging. Eur. J. Neurosci. 9, 1329–39.

Petrides, M., 2005. Lateral prefrontal cortex: architectonic and functional organization. Philos. Trans. R. Soc. Lond. B. Biol. Sci. 360, 781–95. https://doi.org/10.1098/rstb.2005.1631

Petrides, M., Pandya, D.N., 2002. Comparative cytoarchitectonic analysis of the human and the macaque ventrolateral prefrontal cortex and corticocortical connection patterns in the monkey. Eur. J. Neurosci. 16, 291–310.

Petrides, M., Pandya, D.N., 1999. Dorsolateral prefrontal cortex: comparative cytoarchitectonic analysis in the human and the macaque brain and corticocortical connection patterns. Eur. J. Neurosci. 11, 1011–36.

R Core Team, 2016. R: A Language and Environment for Statistical Computing.

Race, E.A., Kuhl, B.A., Badre, D., Wagner, A.D., 2009. The dynamic interplay between cognitive

control and memory., in: Gazzaniga, M.S. (Ed.), The Cognitive Neurosciences. MIT Press, Cambridge, MA, USA; London, UK, pp. 705–724.

Ramnani, N., Owen, A.M., 2004. Anterior prefrontal cortex: insights into function from anatomy and neuroimaging. Nat. Rev. Neurosci. 5, 184–94. https://doi.org/10.1038/nrn1343

Reynolds, J.R., O'Reilly, R.C., Cohen, J.D., Braver, T.S., 2012. The function and organization of lateral prefrontal cortex: a test of competing hypotheses. PLoS One 7, e30284. https://doi.org/10.1371/journal.pone.0030284

Roebroeck, A., Formisano, E., Goebel, R., 2005. Mapping directed influence over the brain using Granger causality and fMRI. Neuroimage 25, 230–42. https://doi.org/10.1016/j.neuroimage.2004.11.017

Saur, D., Kreher, B.W., Schnell, S., Kümmerer, D., Kellmeyer, P., Vry, M.-S., Umarova, R., Musso, M., Glauche, V., Abel, S., Huber, W., Rijntjes, M., Hennig, J., Weiller, C., 2008. Ventral and dorsal pathways for language. Proc. Natl. Acad. Sci. U. S. A. 105, 18035–40. https://doi.org/10.1073/pnas.0805234105

Schelter, B., Winterhalder, M., Eichler, M., Peifer, M., Hellwig, B., Guschlbauer, B., Lücking, C.H., Dahlhaus, R., Timmer, J., 2006. Testing for directed influences among neural signals using partial directed coherence. J. Neurosci. Methods 152, 210–9. https://doi.org/10.1016/j.jneumeth.2005.09.001

Scholkmann, F., Kleiser, S., Metz, A.J., Zimmermann, R., Mata Pavia, J., Wolf, U., Wolf, M., 2014. A review on continuous wave functional near-infrared spectroscopy and imaging instrumentation and methodology. Neuroimage 85 Pt 1, 6–27. https://doi.org/10.1016/j.neuroimage.2013.05.004

Schumacher, L. V., Reisert, M., Nitschke, K., Egger, K., Urbach, H., Hennig, J., Weiller, C., Kaller, C.P., 2018. Probing the reproducibility of quantitative estimates of structural connectivity derived from global tractography. Neuroimage 175, 215–229. https://doi.org/10.1016/j.neuroimage.2018.01.086

671 Stokes, M.G., Kusunoki, M., Sigala, N., Nili, H., Gaffan, D., Duncan, J., 2013. Dynamic Coding for
672 Cognitive Control in Prefrontal Cortex. Neuron 78, 364–375.
673 https://doi.org/10.1016/j.neuron.2013.01.039

674 Strangman, G., Boas, D.A., Sutton, J.P., 2002. Non-invasive neuroimaging using near-infrared light.
675 Biol. Psychiatry 52, 679–693. https://doi.org/10.1016/S0006-3223(02)01550-0

676 Swann, N.C., Tandon, N., Pieters, T. a, Aron, A.R., 2013. Intracranial electroencephalography reveals
677 different temporal profiles for dorsal- and ventro-lateral prefrontal cortex in preparing to stop
678 action. Cereb. Cortex 23, 2479–88. https://doi.org/10.1093/cercor/bhs245

679 Takahashi, E., Ohki, K., Kim, D.-S., 2013. Dissociation and convergence of the dorsal and ventral
680 visual working memory streams in the human prefrontal cortex. Neuroimage 65, 488–98.
681 https://doi.org/10.1016/j.neuroimage.2012.10.002

682 Tanji, J., Hoshi, E., 2008. Role of the lateral prefrontal cortex in executive behavioral control. Physiol.
683 Rev. 88, 37–57. https://doi.org/10.1152/physrev.00014.2007

684 Taren, A.A., Venkatraman, V., Huettel, S.A., 2011. A parallel functional topography between medial
685 and lateral prefrontal cortex: evidence and implications for cognitive control. J. Neurosci. 31,
686 5026–31. https://doi.org/10.1523/JNEUROSCI.5762-10.2011

687 Thompson-Schill, S.L., D'Esposito, M., Aguirre, G.K., Farah, M.J., 1997. Role of left inferior
688 prefrontal cortex in retrieval of semantic knowledge: a reevaluation. Proc. Natl. Acad. Sci. U. S.
689 A. 94, 14792–14797. https://doi.org/10.1073/pnas.94.26.14792

690 Voytek, B., Kayser, A.S., Badre, D., Fegen, D., Chang, E.F., Crone, N.E., Parvizi, J., Knight, R.T.,
691 D'Esposito, M., 2015. Oscillatory dynamics coordinating human frontal networks in support of
692 goal maintenance. Nat. Neurosci. 18, 1318–24. https://doi.org/10.1038/nn.4071

693 Wendelken, C., Chung, D., Bunge, S.A., 2012. Rostrolateral prefrontal cortex: domain-general or
694 domain-sensitive? Hum. Brain Mapp. 33, 1952–63. https://doi.org/10.1002/hbm.21336

695